Spin-resolved electron-phonon coupling in FeSe and KFe_2Se_2

Timur Bazhirov and Marvin L. Cohen

Department of Physics, University of California at Berkeley, Berkeley, California 94720, USA and
Materials Sciences Division, Lawrence Berkeley National Laboratory, Berkeley, California 94720, USA

(Received 16 May 2012; revised manuscript received 24 September 2012; published 16 October 2012)

The effect of the static magnetic moments of iron on electron-phonon interactions in layered FeSe and KFe_2Se_2 is studied. First-principles techniques based on the pseudopotential density functional approach and the local spin density approximation are utilized to calculate the band structures, phonon dispersions, and electron-phonon coupling properties. Our results indicate that the introduction of iron magnetic moments leads to significant changes in electronic structure induced by Fe 3*d* states near the Fermi level, to phonon frequency softening for several vibrational modes, and to a dramatic increase in electron-phonon coupling for specific modes. The increase in Brillouin-zone-averaged coupling is about twofold. Our estimates of superconducting transition temperatures based on the McMillan equation yield values closer to experimental results for the spin-resolved case. However, these values are not large enough to explain the observed transition temperature.

DOI: 10.1103/PhysRevB.86.134517 PACS number(s): 71.38.−k, 74.70.Xa, 63.20.kd

I. INTRODUCTION

One of the simplest iron-based superconducting compounds, FeSe has many characteristic properties of this group and thus can potentially be considered as a model system for studying the electron pairing mechanism for iron-based superconductors. At ambient conditions, FeSe has a transition temperature T_c of 8 K for slightly Se-deficient samples, and the presence of superconductivity is extremely sensitive to sample stoichiometry.[1,2] When pressure is applied the T_c grows to 27 K at 1.5 GPa and to 37 K at 9 GPa,[3,4] perhaps suggesting that lattice vibrations are playing an important role in the superconductivity. Antiferromagnetic spin fluctuations are reported to be strong, although no static long-range magnetic order was found for the superconducting phase.[5] Recent reports also suggest the presence of a nodal gap[6] and an unconventional value for the isotope effect parameter.[7] Studies of FeSe monolayer systems on different substrates show significant sensitivity to interface effects and also give some signs of the presence of superconductivity above 77 K.[8,9]

A number of intercalated FeSe compounds were experimentally prepared using alkali, alkaline-earth, or rare-earth metals as intercalants.[10,11] The resulting T_c is raised to above 30 K at ambient pressure. Of particular interest is the simultaneous presence of superconductivity and antiferromagnetism in these systems and its relation to the iron vacancy ordering.[12,13] NMR experiments suggest that spin fluctuations are weak.[14] Raman spectra exhibit phonon anomalies indicative of a rather specific type of electron-phonon coupling[15] In addition, high-pressure measurements are indicative of extreme sensitivity to the nature of defects.[16] All the above give evidence for the importance of taking the effects of lattice vibrations into account when studying the possible mechanism for superconductivity in selenides.

Theoretical findings, alongside angle-resolved photoemission spectroscopy and de Haas–van Alphen experiments, help to determine the most probable nature of the Fermi surface geometry,[17,18] even though the availability of good-quality crystalline samples limits these studies. Theoretical predictions suggest that for FeSe, the Fermi surface has pockets at points Γ and *M* of the Brillouin zone (BZ). The intercalated compounds tend not to have the zone-centered pockets, according to both theoretical and experimental findings.[19,20] The latter fact does not support the widely accepted $s_\pm$ superconducting gap structure model.[21,22] Pioneering first principle studies for 1111 and 122 compounds have addressed the effect of changes in electronic structure depending on the Fe magnetic moment and spin configuration.[23,24] Magnetoelastic coupling was found to be profound and vibrational properties and electron-phonon interaction strength were studied previously for 1111 and 122 systems in Ref. 25. Electron-phonon coupling calculations without including spin-polarization effects yield values too low to account for the experimentally observable transition temperature within the standard McMillan-Eliashberg approach.[19] When iron magnetic moments are included into the calculation, a significant increase is seen for the 122 and 111 systems.[26] Significant phonon softening was also reported for FeSe.[27] Finally, it is worth mentioning here that many-body dynamical mean-field theory results have proposed the presence of rather strong electronic correlation.[28]

In this work we study the influence of the static magnetic moments of iron on the electronic structure and vibrational and electron-phonon coupling properties of layered iron chalcogenide systems including bulk FeSe and K-intercalated FeSe. For the spin-resolved study we choose the checkerboard and the striped antiferromagnetic configurations (vibrational properties have been studied for FeSe only in the striped case). The latter is seen experimentally for many iron superconductors in the ordered state, while the former can be relatively simply approached in calculations. We utilize an approach based on first-principles pseudopotential density functional theory and the local spin density approximation. Our results show significant changes in the electronic structure and clear evidence of phonon softening when spin is considered. Both of these effects lead to a doubling of the electron-phonon coupling for checkerboard spin-resolved configurations. Electron-phonon matrix elements for a particular phonon mode of A_{1g} symmetry show a dramatic increase as well. Superconducting T_c estimates were made based on the Eliashberg spectral

 ©2012 American Physical Society

function analysis and the McMillan equation.[29] The T_c values for the checkerboard spin-resolved case are much higher than in the case when spin is not included, but the values are still one order of magnitude lower then experimental results.

II. CALCULATION DETAILS

The electronic properties are calculated using the generalized gradient approximation (GGA) to density functional theory[30,31] within a plane-wave pseudopotential scheme.[32,33] Phonon dispersions are calculated through density-functional perturbation theory.[34] The electron-phonon coupling matrix elements, total coupling parameter, and transition temperatures are obtained using the standard McMillan-Eliashberg-based approach.[35]

A cutoff of 80 Ry is used for the wave function expansion, and a 560 Ry cutoff for charge densities. Brillouin-zone sampling is performed on a $64 \times 64 \times 16$ momentum k-space grid for electronic integration and an $8 \times 8 \times 8$ q-space grid for dynamical matrices calculations.

For the purpose of future analysis, the expression for the electron-phonon matrix element is

$$M^{[\nu]}_{\vec{k},\vec{k}+\vec{Q}} = \left(\frac{\hbar}{m\omega_{\vec{Q},\nu}}\right)^{1/2} \langle \vec{k}|\delta_\nu V|\vec{k}+\vec{Q}\rangle. \quad (1)$$

Here $\vec{Q}$ is the phonon scattering vector, $\langle\vec{k}|$ is the initial electronic eigenstate, $|\vec{k}+\vec{Q}\rangle$ is the final electronic eigenstate, and $\delta_\nu V$ is the phonon perturbation operator for a particular mode ν. A more detailed explanation of the electron-phonon coupling calculation technique can be found in Ref. 35.

III. RESULTS

The results given in this section are for relaxed configurations, where the lattice constants were optimized to minimize the forces on the atoms. The reason for this approach is to study phonon properties more precisely by using a near-equilibrium configuration. Otherwise negative phonon frequencies emerge as artifacts. For FeSe, in the nonmagnetic and checkerboard spin-resolved configurations, we use a four-atom unit cell. For the striped spin-resolved configuration a unit cell twice as large with eight atoms is used. For KFe_2Se_2 we use a ten-atom unit cell for all calculations. For FeSe we find the striped spin arrangement to be 24 mRy lower in energy than the nonmagnetic one, and 6 mRy lower than the checkerboard spin pattern. The KFe_2Se_2 unit cell in the checkerboard configuration is 42 mRy lower in total energy than the nonmagnetic one, and 9 mRy lower than the striped configuration.

First, we analyze the effect of the iron magnetic moments on the electronic structure of FeSe. It can be seen from Figs. 1 and 2 that the nonmagnetic band structure for bulk FeSe is similar to what was originally obtained in Ref. 19. The spin-resolved band structure has two main differences: there are only two bands instead of five that cross the Fermi level, and one of the two has a very small energy bandwidth. These two differences can also be clearly seen in the density of states (DOS) plots in the figures mentioned. The total DOS has a peak right at the Fermi level for the spin-polarized case,

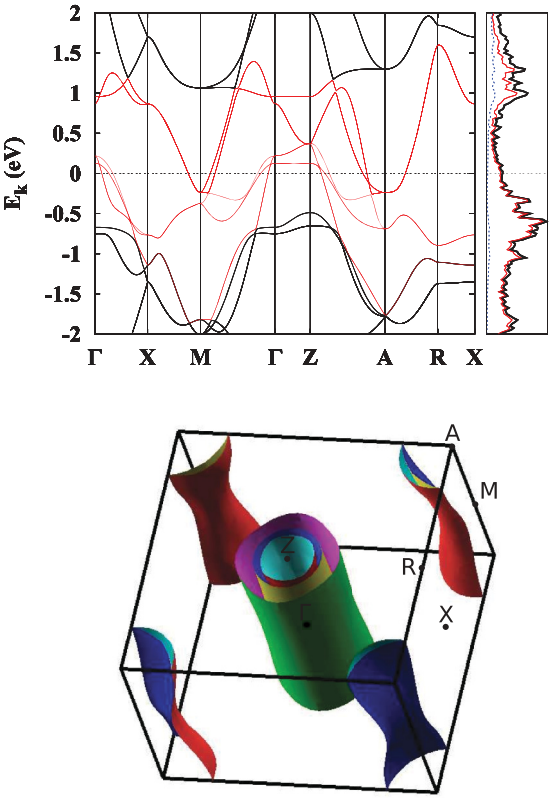

FIG. 1. (Color online) Top: Electronic band structure of FeSe for the non-spin-polarized case. Brighter colored bands are those crossing the Fermi level. To the right the corresponding projected densities of states (in states/eV, from 0 to 12) are plotted for all atoms (black solid), Fe $3d$ states (red solid), and Se (blue dashed). Bottom: The corresponding Fermi surface. The high-symmetry points are given and correspond to the points along the band structure plot on top.

whereas the width of the peak is smaller and its position is not correlated with E_F for the nonpolarized configuration. The partial density of states around the Fermi level is dominated by Fe $3d$ states in both cases. These changes in electronic structure significantly affect the shape of the Fermi surface. The overall shape with electron pockets centered at M and hole pockets at Γ is modified. The pockets at M are still present, whereas the hole pockets are now centered at Z.

The electronic properties of the striped antiferromagnetic spin-resolved configuration are summarized in Fig. 3. Calculation of the striped spin arrangement requires twice as many atoms in a unit cell, so the Fermi surface is a fraction of the one examined in the nonmagnetic and checkerboard antiferromagnetic configurations. The Fermi surface is formed by two bands. The peak in the total density of states is located somewhat below the Fermi level and thus does not play a large role for the electron-phonon interaction. The general shape of the Fermi surface has one cylindrical pocket at the Γ point and two smaller satellite pockets next to it. The satellite pockets are aligned with the stripe direction. The pocket at Γ for the striped configuration's reduced BZ would produce pockets at both Γ and M for the BZ for non-spin-resolved and checkerboard spin systems.

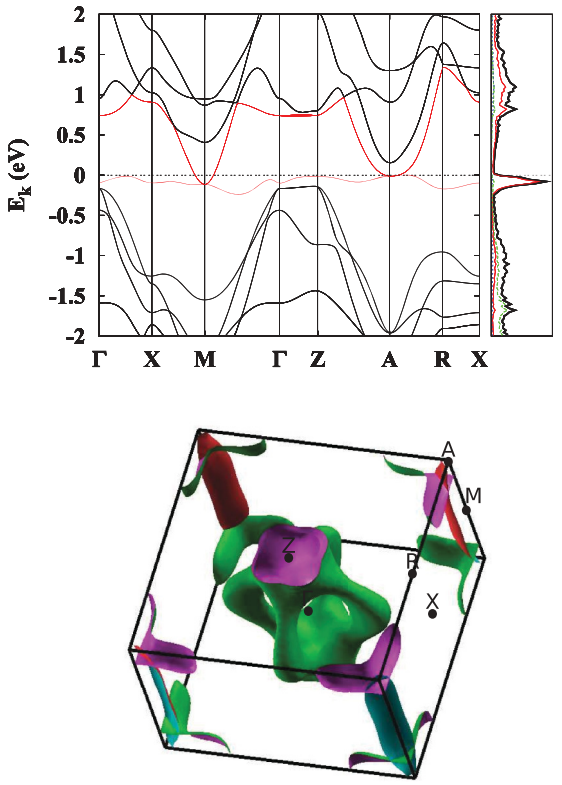

FIG. 2. (Color online) Top: Electronic band structure of FeSe for the checkerboard spin-polarized case. Brighter colored bands are those crossing the Fermi level. To the right the corresponding projected densities of states (in states/eV, from 0 to 11) are plotted for all atoms (black solid), Fe 3*d* up states (red solid), Fe 3*d* down states (green dashed), and Se (blue dot-dashed). Bottom: The corresponding Fermi surface.

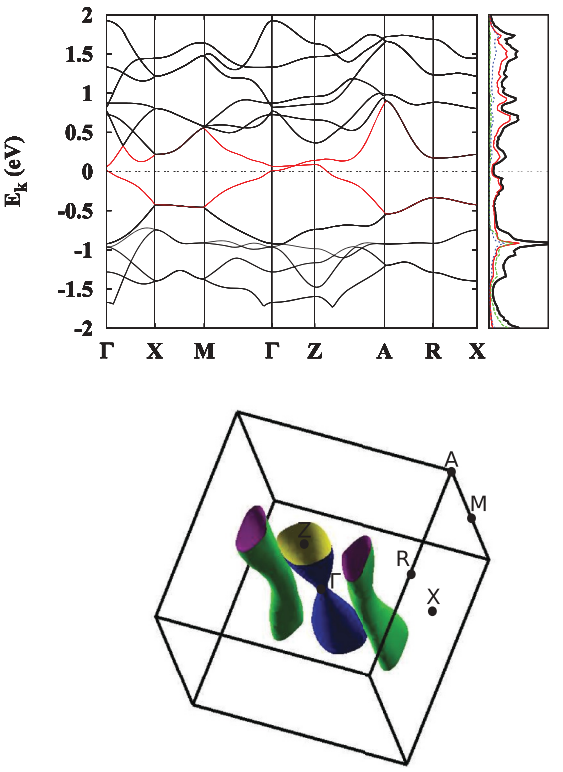

FIG. 3. (Color online) Top: Electronic band structure of FeSe for the striped spin-polarized case. Brighter colored bands are those crossing the Fermi level. To the right the corresponding projected densities of states (in states/eV, from 0 to 15) are plotted for all atoms (black solid), Fe 3*d* up states (red solid), Fe 3*d* down states (green dashed), and Se (blue dot-dashed). Bottom: The corresponding Fermi surface. Note that, even though the striped spin configuration has a different BZ (rotated by $\pi/2$ and scaled by $\sqrt{2}$ in the k_x and k_y directions), we use the conventional cell, so the symmetry points on the wave vector path along the x axis have the same coordinates when expressed in terms of reciprocal lattice vectors as for the nonmagnetic and checkerboard BZs. The stripe direction is toward the given X point. The Y point corresponding to a direction perpendicular to the stripe is not shown.

Secondly, we analyze the effect of the iron magnetic moments on the electronic structure of KFe_2Se_2. In Figs. 4 and 5 the nonmagnetic and checkerboard spin-resolved band structures for KFe_2Se_2 are given. Again, the spin-resolved band structure has fewer energy bands crossing the Fermi level and their energy bandwidths are narrowed. The same two differences can be seen when comparing the partial density of states (PDOS) plots. As in the case of FeSe, the total DOS has an Fe-3*d*-state-induced peak very close to the Fermi level for the spin-polarized case. Generally, we can state that the Fe 3*d* states are becoming more localized in energy when the spins are included. The way the shape of the Fermi surface evolves can also be seen from the above figures. Overall, the Fermi surface of KFe_2Se_2 for the spin-resolved case does not have pockets at Γ and is much better nested (it has regions that amplify scattering possibilities for a particular wave vector; see Ref. 35, for example, for more explanation of the nesting function). Further discussion is presented in Sec. IV.

The electronic properties of the striped antiferromagnetic spin-resolved configuration for KFe_2Se_2 are given in Fig. 6. We used a unit cell containing ten atoms to study striped spin arrangement; however, the shape of the BZ is different than for the configurations mentioned in the previous paragraph. As can be seen in the figure, the striped spin arrangement has a band structure similar to that of a hole-doped semiconductor with a rather small gap of a few hundreds of meV. The Fermi surface has two regions formed by two bands, one of which shows a significant degree of nesting. No pockets are present at the center of the BZ at Γ. On the DOS plot a sharp peak induced by Fe 3*d* states can be seen at about 0.7 eV below the Fermi level.

Third, the phonon dispersions are given in Figs. 7, 8, and 9. For FeSe it can be clearly seen that when we compare non-spin- and spin-resolved cases, there is a significant degree of softening present for the particular phonon mode having A_{1g} symmetry. This phonon branch has frequencies around 250–260 cm^{-1} for $\vec{q}$ between Γ-Z and Γ-X when no spin is considered. These frequencies move to below 200 cm^{-1} when the iron magnetic moments are included in the calculation. Other phonon modes are affected in a similar way, exhibiting overall softening, although significantly smaller in magnitude. The phonon density of states plots illustrate increased weight in the lower-frequency region, and the same conclusion is true for the electron-phonon spectral function. The A_{1g} phonons yield the largest electron-phonon coupling values as well.

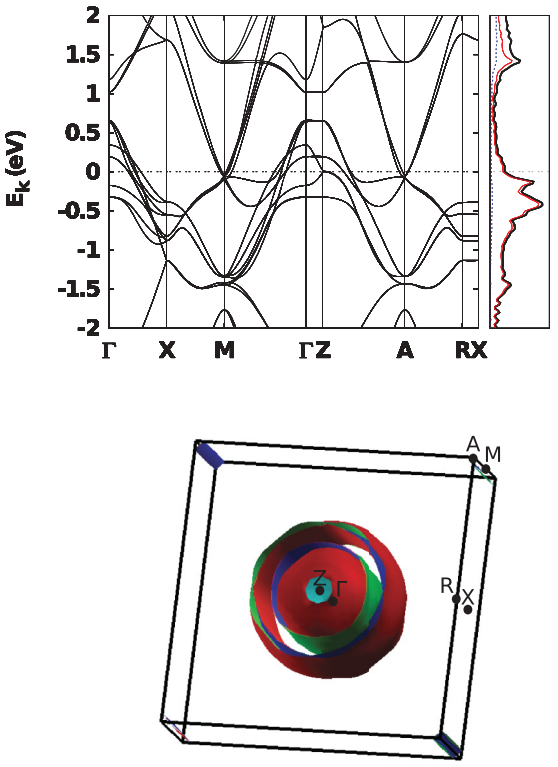

FIG. 4. (Color online) Top: Electronic band structure of KFe_2Se_2 for the non-spin-polarized case. To the right the corresponding projected densities of states (in states/eV, from 0 to 30) are plotted for all atoms (black solid), Fe 3*d* states (red solid), and Se (blue dashed). Bottom: The corresponding Fermi surface.

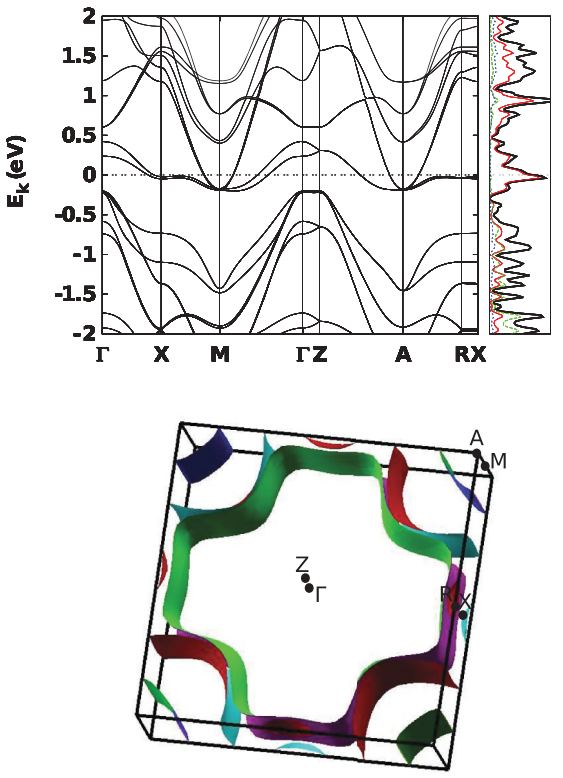

FIG. 5. (Color online) Top: Electronic band structure of KFe_2Se_2 for the checkerboard spin-polarized case. To the right the corresponding projected densities of states (in states/eV, from 0 to 15) are plotted for all atoms (black solid), Fe 3*d* up states (red solid), Fe 3*d* down states (green dashed), and Se (blue dot-dashed). Bottom: The corresponding Fermi surface.

The phonon dispersions for FeSe in the striped spin configuration show some signs of softening, as can be seen from the density of states plot. However, the degree of this softening is not large. A peak in the Eliashberg function at about 200 cm^{-1} arises from electron-phonon coupling to the B_{3g} mode, which seems to account for about 40% of the total coupling.

The phonon dispersion relations for KFe_2Se_2 exhibit similar behavior. A comparison between spin-resolved and non-spin-resolved cases shows a general softening, which is most evident for $\vec{q}$ between Γ-Z and Γ-X. Vibrational states in the 100–150 cm^{-1} region are lowered to below 100 cm^{-1}. The latter can be derived from the comparison between the phonon density of states plots, providing evidence for increasing numbers of phonons in the low-frequency region when spins are included. The spectral weight shift to lower frequencies is also present in the electron-phonon spectral function plots.

The electron-phonon coupling values, averaged over the Brillouin zone, estimated values of the superconducting transition temperature, the density of states at the Fermi level, the average electron-phonon matrix element value, and the logarithmic averaged frequency are summarized in Table I. The T_c corresponding to the calculated electron-phonon coupling parameter is obtained using the modified McMillan equation.[29] The degree of BZ sampling used suggests that the average coupling value λ is precise to within an error of 10%–15%. On the other hand, precise calculation of the Eliashberg spectral function needs better sampling, so the given values of the spectral function frequency moment—$\omega_{\log}$—are rough estimates. As we see, λ increases from 0.15 for non-spin-resolved FeSe to 0.39 for the checkerboard spin-resolved configuration, and correspondingly from 0.19 to 0.34 for KFe_2Se_2. This leads to a T_c of 1.1 K and 0.2 K when iron moments are included in the calculation, and for practically zero values in the opposite case. The striped spin-resolved FeSe case has a coupling value of 0.16 and thus zero T_c. We show that using the commonly used value of the Coulomb repulsion parameter $\mu^* = 0.1$ even for the checkerboard spin-resolved case we do not achieve consistency with the experimentally measured superconducting transition of 8 K for FeSe.[1] The T_c estimates for spin-resolved KFe_2Se_2 are also far away from the experimental value of 32 K.[10]

IV. DISCUSSION

Currently, for the cases of the iron-based and copper oxide superconductors there is no consensus regarding the mechanism of electron pairing. In the iron-based compounds, a widely accepted picture is that the itinerant electronic system has a weak but substantial interaction with the significantly localized magnetic moments and charges of the Fe atoms.[28,36–38] Thus the degree of electronic correlation may be strong enough to be beyond the limits of applicability of the bare local density (LDA) and generalized gradient (GGA) approximations. In addition, the fact that no long-range magnetic order is usually

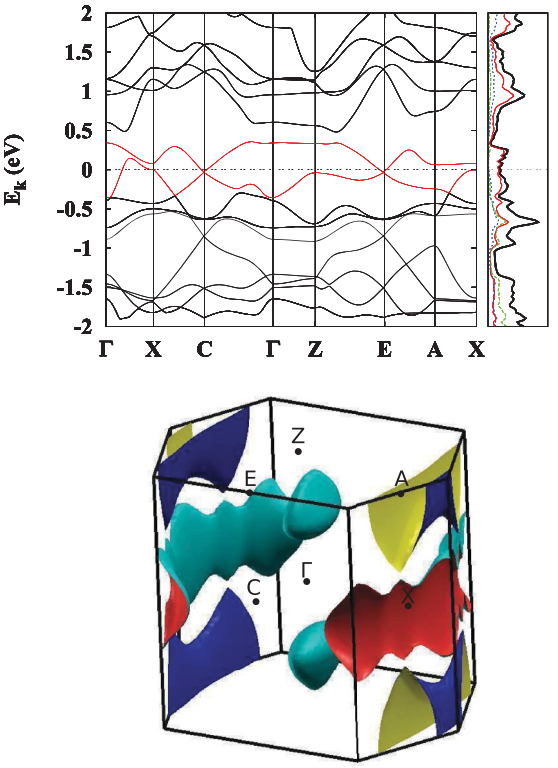

FIG. 6. (Color online) Top: Electronic band structure of KFe_2Se_2 for the striped spin-polarized case. Brighter colored bands are those crossing the Fermi level. To the right the corresponding projected densities of states (in states/eV, from 0 to 12) are plotted for all atoms (black solid), Fe 3*d* up states (red solid), Fe 3*d* down states (green dashed), Se (blue dot-dashed), and K (purple dot-dashed). Bottom: The corresponding Fermi surface. Note that the striped spin configuration has a monoclinic BZ due to stripe-induced lattice distortion. We use corresponding symmetry points on the wave vector path along the *x* axis that have the same coordinates when expressed in terms of reciprocal lattice vectors as for the nonmagnetic and checkerboard BZs. The stripe direction is toward the given *X* point.

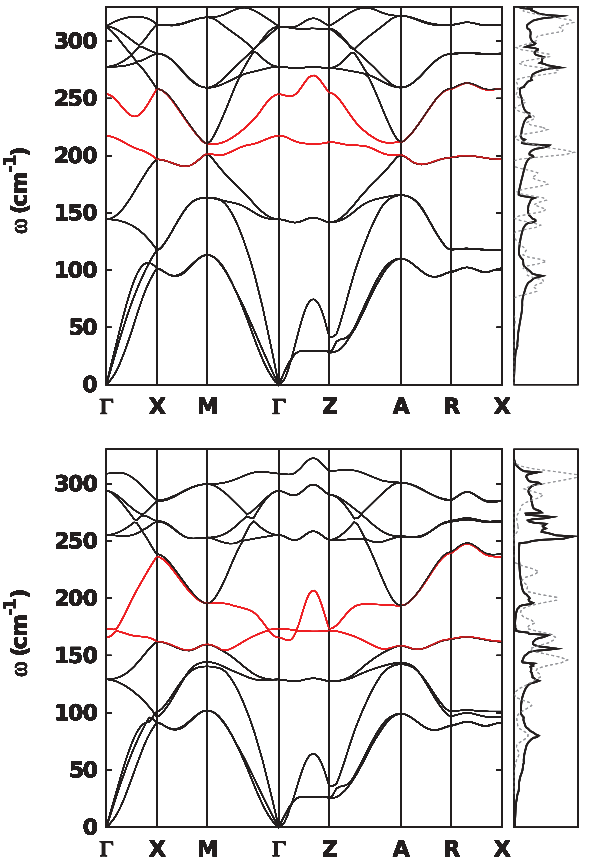

FIG. 7. (Color online) Phonon dispersions of FeSe for the non-spin-polarized (top) and the checkerboard spin-polarized (bottom) configurations. The phonon density of states (solid) and Eliashberg spectral function (dashed) are given to the right (in states/cm^{-1}, from 0 to 0.2, for the nonmagnetic and in states/cm^{-1} multiplied by 2, from 0 to 0.4, for the spin-resolved configuration). Bands showing the largest degree of softening are shown in red (brighter) color to guide the eye.

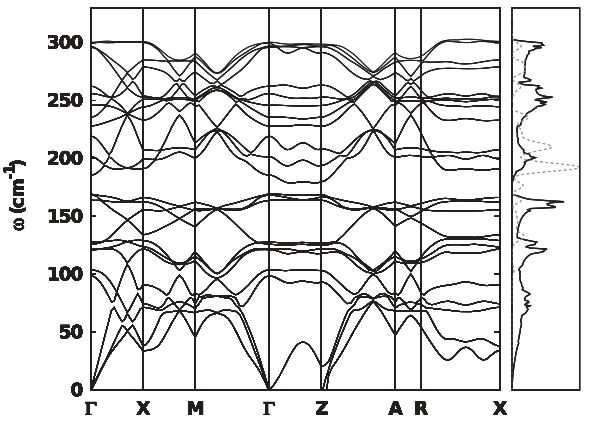

FIG. 8. Phonon dispersions of FeSe for the striped spin-polarized configuration. Phonon density of states (solid) and Eliashberg spectral function (dashed) are given to the right (in states/cm^{-1} multiplied by 1.5 for the PDOS, from 0 to 0.3). Note that, even though the striped spin configuration has a different BZ, the symmetry points on the wave vector path along the *x* axis have the same coordinates when expressed in terms of reciprocal lattice vectors as for the nonmagnetic and checkerboard BZs, so the symbols remain the same.

seen in these systems experimentally implies that the spin-resolved LDA and GGA may not model the experimental state accurately either.[5,37] The cases of non-spin-resolved and spin-resolved local spin density approximation (LSDA) and GGA calculations can thus be treated as the extremes, and the real experimental situation may be somewhere between the two. The electronic structure properties of iron superconductors are widely believed to be predicted well by the LDA without the treatment of spins. This appears to be justified by substantial agreement with experimental results on the Fermi surface shapes at least for 1111 and 122 compounds.[36,37,39–42] On the other hand, properties such as equilibrium lattice constants, for example, are better described within the spin-resolved approximation.[20] Therefore in this work we present a deliberate comparison of the two approaches, considering both electronic and vibrational characteristics. The questions about the destruction of magnetic order inside the superconducting phase and the presence of phase separation into a nonmagnetic superconducting phase and a magnetic semiconducting phase are still open for KFe_2Se_2.[43] Also the presence of strong

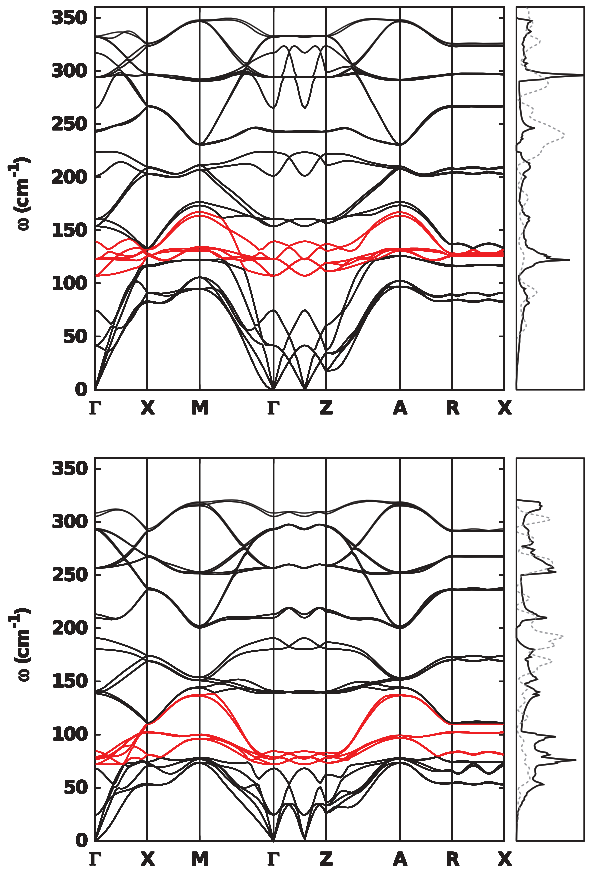

FIG. 9. (Color online) Phonon dispersions of KFe_2Se_2 for the non-spin-polarized (top) and the checkerboard spin-polarized (bottom) configurations. The phonon density of states (solid) and Eliashberg spectral function (dashed) are given to the right (in states/cm^{-1} multiplied by 1.5 for the nonmagnetic and in states/cm for the spin-resolved configuration, from 0 to 0.5). Bands showing the largest degree of softening are shown in red (brighter) color to guide the eye.

spin fluctuations has been experimentally reported for FeSe.[5] Thus knowledge of the difference between magnetic and nonmagnetic electronic and vibrational properties for both of these compounds is necessary. It would also be interesting to study the effect of nonstoichiometry on the electronic and vibrational properties of FeSe compounds, but doing so is rather complicated since the experimental shift in stoichiometry is rather small.

We compare the band structures and Fermi surfaces (FSs) first. Here and below we refer to the non-spin-resolved calculations as LDA and to spin-resolved ones as LSDA calculations for brevity, even though the actual exchange-correlation functionals used are GGA based. As was mentioned earlier, the 3d states of iron are more localized in energy at the Fermi level for the LSDA case. This leads to the differences in the FS shapes. Since there are no experimental data available for direct comparison for pure FeSe, no conclusion can be made about which method works best. Nevertheless, some features of the LSDA FS can still be expected to be present in experiments. In particular, the fact that the FS is better nested could be important. For KFe_2Se_2, experimental findings[18] show no pockets at Γ, which is in agreement with the Fermi surface we find for the spin-resolved case. The fact that our LDA Fermi surface is different from what was obtained in Ref. 20 might arise from the necessity to use a relaxed configuration to obtain a dynamically stable structure in this work. In general, we note here that the spin-resolved calculations give better results for equilibrium lattice constants for both compounds (about 1% smaller than the experimental value for FeSe, and 3% smaller for KFe_2Se_2) and are in agreement with currently available experimental data for the Fermi surfaces. It is also worth mentioning that if the Fermi level is moved slightly, the Fermi surface shape for FeSe can undergo significant changes because of the high degree of Fe 3d state localization in energy in the spin-resolved case.

TABLE I. Summary of the electronic and electron-phonon interaction related parameters obtained in this work. We show the total coupling strength λ, as well as the Fe magnetic moment $|\mu|$ (in Bohr magnetons), the density of states at the Fermi level $N(E_F)$ (in states/Ry divided by the number of iron atoms in the unit cell), the logarithmic average frequency (in K), and the average electron-phonon matrix element squared $\langle M^2\rangle$ (arbitrary units). The superconducting transition temperature (T_c, in K) is estimated using the Allen-Dynes formula (Ref. 29) with the Coulomb parameter μ^* given above.

Material	$\lvert\mu\rvert$	$N(E_F)$	$\omega_{\log}$	λ	$\langle M^2\rangle$	$T_c(\mu^*=0.1)$
FeSe		10.5	250	0.15	0.4	0.0
FeSe (checkerboard)	2.2	13.5	280	0.39	0.7	1.1
FeSe (striped)	2.6	6.5	280	0.16	0.4	0.0
KFe_2Se_2		16.5	240	0.18	0.9	0.0
KFe_2Se_2 (checkerboard)	2.6	18.2	180	0.34	1.1	0.2
KFe_2Se_2 (stripe)	2.8	9.5				

To test the importance of the change introduced to the nesting, we calculate the electron-phonon matrix elements averaged over Q_z [see Eq. (1)],

$$M = \frac{1}{N_{Q_z}} \sum_{Q_z} M^{[\nu]}_{\vec{k},\vec{k}+\vec{Q}}, \tag{2}$$

and then analyze the difference between the spin-resolved squared matrix elements and non-spin-resolved ones,

$$\Delta M^2 = M^2_{SP} - M^2_{NS}. \tag{3}$$

Color maps of the differences in checkerboard spin-resolved and non-spin-resolved q_z-averaged matrix elements squared, $\Delta M^2(q_x,q_y)$, are plotted in Fig. 10. It can be seen that for FeSe at $|Q(x,y)| = (0.5\ 0.5)$ and for KFe_2Se_2 at $|Q(x,y)| = (0.0\ 0.5)$, the ΔM^2 are significantly amplified for spin-resolved configuration. A closer look at the corresponding Fermi surface shapes confirms that nesting opportunities do increase for those two wave vectors when the spin treatment is included. Thus, we can conclude that nesting does play a significant role in the overall increase of the electron-phonon coupling.

Phonon softening serves as another important factor affecting the electron-phonon coupling. We again emphasize the fact that there are specific phonon modes of A_{1g} symmetry that are affected the most. This means that, when the spin treatment is turned on, the spatial structure of electronic states is affected

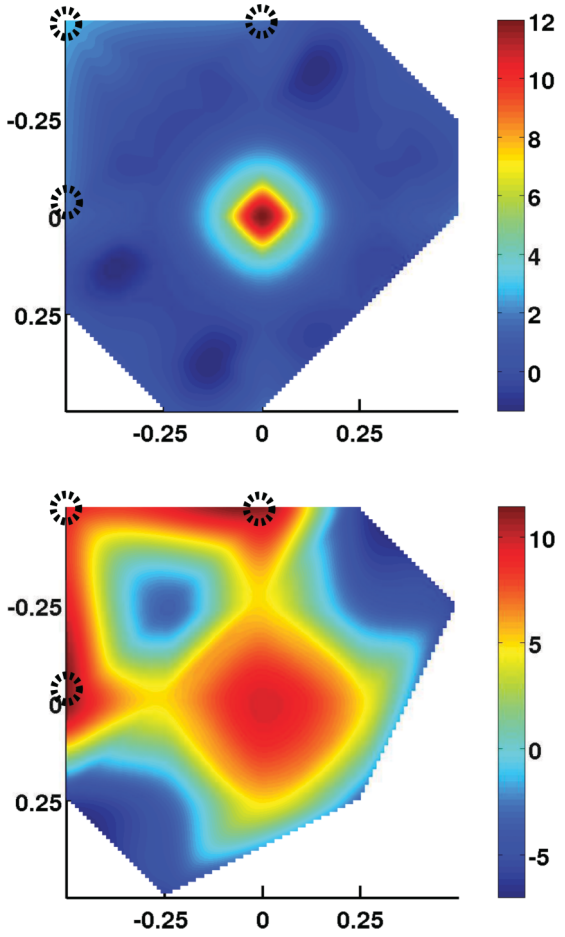

FIG. 10. (Color online) Color map of the differences in matrix elements δM^2 between the checkerboard spin-resolved and non-spin-resolved cases [according to (3)] given for FeSe (top) and KFe_2Se_2 (bottom). The values on the x and y axes are in units of $2\pi/a$, and on the z axis in arbitrary units. The points (0.0 0.5) and (0.5 0.5) are shown using dashed circles.

in such a way that it favors the A_{1g} phonon softening. Visual analysis of the shapes of electronic states at the Fermi level tends to confirm that observation. It is also worthwhile to notice that for the spin-resolved case, 90% of the total coupling at Γ comes from the A_{1g} mode, whereas the latter is responsible for only 20% for the non-spin-resolved case. This dramatic increase suggests that the phonon perturbation operator also undergoes significant changes in its shape that strongly favor the above mentioned symmetry.

The chalcogen or pnictogen height is an important parameter reflecting the superconducting properties of iron-based compounds, as has been previously noted.[36] The relative behaviors of FeSe and KFe_2Se_2 in our calculations can be analyzed utilizing this picture. For the checkerboard LSDA, which gives better agreement with experiment for the structural parameters, the relaxed chalcogen height is 1.41 and 1.38 Å for FeSe and KFe_2Se_2, respectively. Since the latter compound has smaller average coupling values and experiments show a rapid increase of T_c with pressure,[3,4] we argue that the optimal chalcogen height could be somewhere between the two values stated above, at least for the electron-phonon-interaction-based contribution to the pairing mechanism.

To sum up how the results of this work can contribute to the overall understanding of the mechanism of superconductivity in iron-based superconductors, we state the following. There exists a widely accepted belief that the nature of superconducting pairing is not entirely between electrons and phonons. The most recent argument in favor of this belief, although for cuprates, is provided by the optical spectroscopy measurements of the spectral function in Ref. 44. Our findings confirm this picture. Nevertheless, we show that for the extreme case when static magnetic moments of iron can coexist with superconductivity, the Migdal-Eliashberg theory would predict much higher coupling and transition temperatures closer to the experimental values then were previously found for nonmagnetic systems.

V. CONCLUSION

We investigated the electron-phonon interactions in layered FeSe and KFe_2Se_2 from first principles by considering the effects of inclusion of static magnetic moments of Fe atoms on electronic, vibrational, and wave-vector-dependent electron-phonon coupling parameters. We find that the $3d$ states of iron are localized more in energy space for the spin-resolved case. The latter leads to important changes in the band structures and Fermi surfaces. The phonon frequencies and electron-phonon coupling are seen to be significantly affected by the changes in electronic structure as well. The shape of the Fermi surface is shown to play an important role. We explain the mechanism by which the electronic structure change induces an enhancement in the electron-phonon coupling and show that it is mainly due to the nesting-related amplification of the electron-phonon matrix elements in specific regions of the BZ.

Our calculation of electron-phonon coupling for spin-resolved configurations in this work provides another way to estimate superconducting transition temperatures. The total electron-phonon coupling values show around a twofold increase (from 0.15 to 0.39 for FeSe, and from 0.19 to 0.34 for KFe_2Se_2) when a checkerboard spin pattern is introduced. We find estimates of T_c based on spin-resolved coupling values to be in better agreement with experiment than estimates for non-spin-resolved configurations, although still not large enough to solely explain the superconductivity on the basis of electron-phonon interactions. Perhaps other first-principles approaches, retaining some of the features provided by the ones we implemented in the current work, are necessary to correctly explain the mechanism of superconductivity in iron selenides.

ACKNOWLEDGMENTS

This work was supported by National Science Foundation Grant No. DMR07-05941 and by the Director, Office of Science, Office of Basic Energy Sciences, Division of Materials Sciences and Engineering Division, US Department of Energy under Contract No. DE- AC02-05CH11231. Computational resources have been provided by LBNL. Calculations were performed using the modified QUANTUM-ESPRESSO package.[45] The authors want to personally thank Hyoung Joon Choi for fruitful discussions and careful reading of the manuscript.

[1]F.-C. Hsu, J.-Y. Luo, K.-W. Yeh, T.-K. Chen, T.-W. Huang, P. M. Wu, Y.-C. Lee, Y.-L. Huang, Y.-Y. Chu, D.-C. Yan, and M.-K. Wu, Proc. Natl. Acad. Sci. USA **105**, 14262 (2008).
[2]T. M. McQueen, Q. Huang, V. Ksenofontov, C. Felser, Q. Xu, H. Zandbergen, Y. S. Hor, J. Allred, A. J. Williams, D. Qu, J. Checkelsky, N. P. Ong, and R. J. Cava, Phys. Rev. B **79**, 014522 (2009).
[3]S. Medvedev, T. M. McQueen, I. A. Troyan, T. Palasyuk, M. I. Eremets, R. J. Cava, S. Naghavi, F. Casper, V. Ksenofontov, G. Wortmann, and C. Felser, Nat. Mater. **8**, 630 (2009).
[4]Y. Mizuguchi, F. Tomioka, S. Tsuda, T. Yamaguchi, and Y. Takano, Appl. Phys. Lett. **93**, 152505 (2008).
[5]T. Imai, K. Ahilan, F. L. Ning, T. M. McQueen, and R. J. Cava, Phys. Rev. Lett. **102**, 177005 (2009).
[6]C.-L. Song, Y.-L. Wang, P. Cheng, Y.-P. Jiang, W. Li, T. Zhang, Z. Li, K. He, L. Wang, J.-F. Jia, H.-H. Hung, C. Wu, X. Ma, X. Chen, and Q.-K. Xue, Science **332**, 1410 (2011).
[7]R. Khasanov, M. Bendele, K. Conder, H. Keller, E. Pomjakushina, and V. Pomjakushin, New J. Phys. **12**, 073024 (2010).
[8]Q.-Y. Wang, Z. Li, W.-H. Zhang, Z.-C. Zhang, J.-S. Zhang, W. Li, H. Ding, Y.-B. Ou, P. Deng, K. Chang, J. Wen, C.-L. Song, K. He, J.-F. Jia, S.-H. Ji, Y. Wang, L. Wang, X. Chen, X. Ma, and Q.-K. Xue, arXiv:1201.5694.
[9]C.-L. Song, Y.-L. Wang, Y.-P. Jiang, Z. Li, L. Wang, K. He, X. Chen, X.-C. Ma, and Q.-K. Xue, Phys. Rev. B **84**, 020503 (2011).
[10]J. Guo, S. Jin, G. Wang, S. Wang, K. Zhu, T. Zhou, M. He, and X. Chen, Phys. Rev. B **82**, 180520 (2010).
[11]A. Krzton-Maziopa, Z. Shermadini, E. Pomjakushina, V. Pomjakushin, M. Bendele, A. Amato, R. Khasanov, H. Luetkens, and K. Conder, J. Phys.: Condens. Matter **23**, 052203 (2011).
[12]Z. Shermadini, A. Krzton-Maziopa, M. Bendele, R. Khasanov, H. Luetkens, K. Conder, E. Pomjakushina, S. Weyeneth, V. Pomjakushin, O. Bossen, and A. Amato, Phys. Rev. Lett. **106**, 117602 (2011).
[13]B. Wei, H. Qing-Zhen, C. Gen-Fu, M. A. Green, W. Du-Ming, H. Jun-Bao, and Q. Yi-Ming, Chin. Phys. Lett. **28**, 086104 (2011).
[14]W. Yu, L. Ma, J. B. He, D. M. Wang, T.-L. Xia, G. F. Chen, and W. Bao, Phys. Rev. Lett. **106**, 197001 (2011).
[15]A. M. Zhang, K. Liu, J. H. Xiao, J. B. He, D. M. Wang, G. F. Chen, B. Normand, and Q. M. Zhang, Phys. Rev. B **85**, 024518 (2012).
[16]B. Wei, H. Qing-Zhen, C. Gen-Fu, M. A. Green, W. Du-Ming, H. Jun-Bao, and Q. Yi-Ming, Chin. Phys. Lett. **28**, 086104 (2011).
[17]T. Qian, X.-P. Wang, W.-C. Jin, P. Zhang, P. Richard, G. Xu, X. Dai, Z. Fang, J.-G. Guo, X.-L. Chen, and H. Ding, Phys. Rev. Lett. **106**, 187001 (2011).
[18]Y. Zhang, L. X. Yang, M. Xu, Z. R. Ye, F. Chen, C. He, H. C. Xu, J. Jiang, B. P. Xie, J. J. Ying, X. F. Wang, X. H. Chen, J. P. Hu, M. Matsunami, S. Kimura, and D. L. Feng, Nat. Mater. **10**, 273 (2011).
[19]A. Subedi, L. Zhang, D. J. Singh, and M. H. Du, Phys. Rev. B **78**, 134514 (2008).
[20]C. Cao and J.-H. Dai, Chin. Phys. Lett. **28**, 057402 (2011).
[21]I. Mazin and J. Schmalian, Physica C **469**, 614 (2009).
[22]I. I. Mazin, Phys. Rev. B **84**, 024529 (2011).
[23]Z. P. Yin, S. Lebègue, M. J. Han, B. P. Neal, S. Y. Savrasov, and W. E. Pickett, Phys. Rev. Lett. **101**, 047001 (2008).
[24]T. Yildirim, Phys. Rev. Lett. **102**, 037003 (2009).
[25]T. Yildirim, Physica C **469**, 425 (2009).
[26]L. Boeri, M. Calandra, I. I. Mazin, O. V. Dolgov, and F. Mauri, Phys. Rev. B **82**, 020506 (2010).
[27]W. Wang, J. Sun, and S. Li, Appl. Phys. Lett. **99**, 082504 (2011).
[28]M. Aichhorn, S. Biermann, T. Miyake, A. Georges, and M. Imada, Phys. Rev. B **82**, 064504 (2010).
[29]P. Allen and R. Dynes, Phys. Rev. B **12**, 905 (1975).
[30]D. M. Ceperley and B. J. Alder, Phys. Rev. Lett. **45**, 566 (1980).
[31]J. P. Perdew and A. Zunger, Phys. Rev. B **23**, 5048 (1981).
[32]J. Ihm, A. Zunger, and M. Cohen, J. Phys. C **12**, 4409 (1979).
[33]N. Troullier and J. L. Martins, Phys. Rev. B **43**, 1993 (1991).
[34]S. Baroni, S. de Gironcoli, A. Dal Corso, and P. Giannozzi, Rev. Mod. Phys. **73**, 515 (2001).
[35]T. Bazhirov, J. Noffsinger, and M. L. Cohen, Phys. Rev. B **82**, 184509 (2010).
[36]H. Oh, J. Moon, D. Shin, C.-Y. Moon, and H. J. Choi, Prog. Supercond. **13**, 65 (2011), arXiv:1201.0237v1.
[37]J. Paglione and R. L. Greene, Nat. Phys. **6**, 645 (2010).
[38]L. Craco and S. Leoni, Europhys. Lett. **92**, 67003 (2010).
[39]D. J. Singh and M. H. Du, Phys. Rev. Lett. **100**, 237003 (2008).
[40]S. Lebègue, Phys. Rev. B **75**, 035110 (2007).
[41]C. Liu, Y. Lee, A. D. Palczewski, J.-Q. Yan, T. Kondo, B. N. Harmon, R. W. McCallum, T. A. Lograsso, and A. Kaminski, Phys. Rev. B **82**, 075135 (2010).
[42]D. H. Lu, M. Yi, S.-K. Mo, A. S. Erickson, J. Analytis, J.-H. Chu, D. J. Singh, Z. Hussain, T. H. Geballe, I. R. Fisher, and Z.-X. Shen, Nature (London) **455**, 81 (2008).
[43]W. Li, H. Ding, P. Deng, K. Chang, C. Song, K. He, L. Wang, X. Ma, J.-P. Hu, X. Chen, and Q.-K. Xue, Nat. Phys. **8**, 126 (2012).
[44]S. Dal Conte, C. Giannetti, G. Coslovich, F. Cilento, D. Bossini, T. Abebaw, F. Banfi, G. Ferrini, H. Eisaki, M. Greven, A. Damascelli, D. van der Marel, and F. Parmigiani, Science **335**, 1600 (2012).
[45]P. Giannozzi *et al.*, J. Phys.: Condens. Matter **21**, 395502 (2009).